Korean Chem. Eng. Res., 53(3), 350-356 (2015)
http://dx.doi.org/10.9713/kcer.2015.53.3.350
PISSN 0304-128X, EISSN 2233-9558

Synthesis of Highly Concentrated ZnO Nanorod Sol by Sol-gel Method and their Applications for Inverted Organic Solar Cells

Solee Kim, Young Chai Kim and Seong-Geun Oh†

Department of Chemical Engineering, Hanyang University,222 Wangsimni-ro, Seongdong-gu, Seoul 133-791, Korea
(Received 31 July 2014; Received in revised form 10 October 2014; accepted 13 October 2014)

Abstract – The effects of the zinc oxide (ZnO) preparing process on the performance of inverted organic photovoltaic cells (OPVs) were explored. The morphology and size of ZnO nanoparticles were controlled, leading to more efficient charge collection from device and higher electron mobility compared with nanospheres. Nanosized ZnO particles were synthesized by using zinc acetate dihydrate and potassium hydroxide in methanol. Also, water was added into the reaction medium to control the morphology of ZnO nanocrystals from spherical particles to rods, and NH_4OH was used to prevent the gelation of dispersion. Solution-processed ZnO thin films were deposited onto the ITO/glass substrate by using spin coating process and then ZnO films were used as an electron transport layer in inverted organic photovoltaic cells. The analyses were carried out by using TEM, FE-SEM, AFM, DLS, UV-Vis spectroscopy, current density-voltage characteristics and solar simulator.

Key words: Inverted Organic Photovoltaics, ZnO Thin Films, Morphology Control, Sol-Gel Method

1. Introduction

ZnO materials have attracted much interest as an n-type semiconductor due to the wide direct bandgap of 3.37 eV and large exciton binding energy of 60 meV at room temperature [1-3]. The ZnO semiconductor has a good transparency, high electron mobility, excellent chemical and thermal stability in different environments, non-toxicity, good adhesion to substrate, and lower cost [4-8]. Also, ZnO is of interest due to availability of low temperature synthesis and the potential for controlling the morphology through simple processing from solution [9]. The widest varieties of ZnO nanostructures have been reported such as nanospheres, nanorods, nanowires, nanorings, nanoneedles, and so on [10-14]. Many methods for the production of ZnO nanostructures have been reported, such as hydrothermal method, sol-gel method, chemical vapor deposition, thermal decomposition, mechanochemical, and electrochemical deposition [15-18]. Synthesized ZnO nanoparticles have been investigated due to their desirable properties and potential technical applications in different areas such as catalyst, gas sensor, optoelectronic device, and solar cells [19-21]. Especially, OPVs are one of the most promising in solar cell field due to their low cost on flexible plastic substrates, light-weight materials, and easy solution-based fabrication. Conventional OPVs can suffer from the degradation of top electrode (Al, Ca, etc.), because a low work function cathode is susceptible to degradation by moisture and oxygen in air. Therefore, an inverted device architecture where the nature of charge collection is reversed was used to improve the device lifetime. In the inverted structure, the interface of ITO/PEDOT:PSS can be avoided and the air-sensitive, low work-function Al can be replaced with air-stable, high-work-function metals such as Au and Ag, as shown in Fig. 1(a). Fig. 1(b) shows the energy level diagram of inverted OPVs with well-matched work function. Also, ZnO inter-layer inserted between the active layer and ITO electrode as an electron transport layer to collect the electrons at the electrode has been successfully applied in inverted OPVs [22]. In addition, limitations such as oxidation of the electrode and degradation under oxygen and moisture for conventional OPVs can be overcome [23].

We synthesized ZnO nanostructures using sol-gel method as an electron transport layer in OPVs and investigated the effect of ZnO morphology on OPV performance. To enhance the power conversion efficiency (PCE), the morphology and size of ZnO nanocrystals were controlled from spherical particles to rods. Nanorods could offer the improved electron transport compared with nanosphere. Moreover, addition of NH_4OH results in the stable dispersion of these ZnO particles improving device performance.

2. Experimental Section

2.1. Materials

Zinc acetate dehydrate (Zn slat, Sigma-Aldrich), potassium hydroxide (KOH, Junsei), and methanol (OCI) were used to prepare the ZnO nanoparticles. Ammonium hydroxide (NH_4OH, Duksan) as stabilizer was used to prevent from gelation after dispersion of ZnO nanorods. For the preparation of ZnO dispersion, 1-butanol (Junsei) was used as an organic medium and 2-(2-methoxyethoxy) acetic

† To whom correspondence should be addressed.
E-mail: seongoh@hanyang.ac.kr
‡This article is dedicated to Prof. Seong-Youl Bae on the occasion of his retirement from Hanyang University.

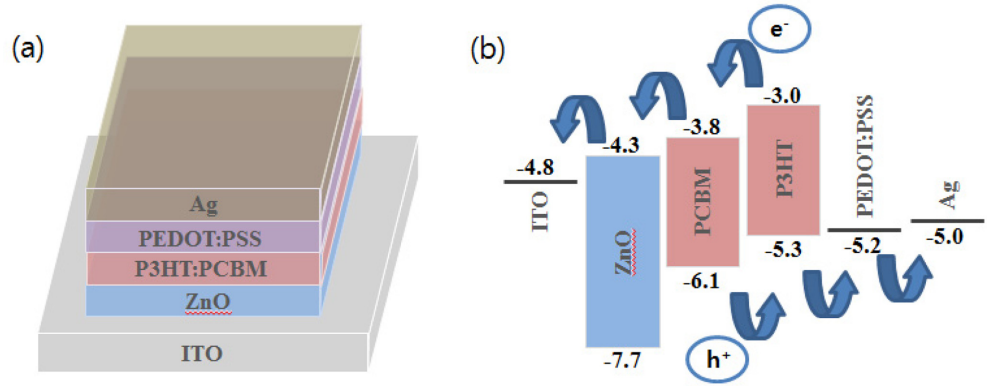

Fig. 1. (a) Device architecture of the inverted OPVs. (b) Schematic energy level diagram of inverted OPVs with a ZnO nanoparticle interlayer. The energies (in eV) are all referenced from the vacuum level.

acid (MEA, Sigma-Aldrich) was used as a dispersant. The slide glasses (Marienfeld-Superior) and the indium tin oxide (ITO)-coated glasses (Geomatec) were used as substrates for the formation of ZnO thin film. Before coating the ZnO thin films, the substrates were cleaned by ultrasonic treatment in acetone (Samchun Company), isopropyl alcohol (IPA, Samchun), and deionized water (Milli-Q Plus system, 18.2 MΩ·cm at 25 °C). For the preparation of active layer, 1,2-dichlorobenzene (Sigma-Aldrich), poly(3-hexylthiophene) (P3HT, Merck), and [6,6]-phenyl-C61-butyric acid methyl ester (PCBM, Merck) were used. Poly (3,4-ethylenedioxythiophene):poly(styrene-sulfonate) (PEDOT:PSS, Heraeus P AI 4083) with Triton X-100 (Sigma-Aldrich Chemical Company) was used for the formation of hole transporting layer. All chemical reagents in this research were analytical grades and used without any further purification.

2-2. Synthesis of ZnO nanospheres and nanorods

2-2-1. ZnO nanosphere synthesis

Spherical ZnO nanoparticles were prepared by using Zn Salt and KOH as starting materials in methanol according to the reported method with some modifications [10]. However, the solvent used for dispersion of ZnO particles was 1-butanol (boiling point: 117.6 °C). In a typical procedure, zinc acetate dehydrate (2.97 g) was dissolved completely in methanol (125 mL) under stirring at 60 °C and then KOH (1.51 g) dissolved completely in methanol (65 mL) at 60 °C was added into zinc acetate dehydrate solution. The molar ratio of Zn salt to KOH was 1 to 2. This mixture was stirred at 60 °C for 3 h and then left to stand at room temperature for 4 h. Precipitate was washed with methanol (100 mL). After the washing step, the methanol was removed by decantation. The washed particles were dispersed in 1-butanol (12 mL) as a solvent for the preparation of ZnO dispersion. The ZnO concentration was in the range 59~83 mg/mL. Then, the MEA (0.04 g) as a ligand was added into the dispersion to improve the dispersion stability of ZnO nanoparticles in 1-butanol. The range of MEA concentration was found to 4~6 wt% with respect to ZnO particles.

2-2-2. ZnO nanorod synthesis

Synthetic process for nanospheres was employed up to the point of the stirring step of the mixture solution at 60 °C before standing for 4 hours. After reaction for 3 h, a small amount of water was added in reaction medium [11]. A different amount of water (1~5 mL) was added to control the size and morphology of ZnO nanorods. This mixture with water was stirred at 60 °C for 3 h and then left to stand at room temperature for 4 h. Washing step of this precipitate and the next process were mentioned in ZnO spheres synthetic process. However, gelation occurred as time passed when more than 4 mL of water was added into ZnO nanorod dispersion. This turbid dispersion became transparent through the addition of NH_4OH or washing process by centrifugation.

2-3. Fabrication of solar cells

Inverted OPV cells composed of ITO/ZnO/P3HT:PCBM/PEDOT:PSS/Ag were fabricated through the following procedure. The ITO substrate was cleaned by sonication with IPA, deionized water, and acetone followed by oxygen plasma treatment. Then, the prepared ZnO dispersions were spin-coated onto the ITO substrates at 3000 rpm for 40 sec and the formed layer was dried at 200 °C for 2 min. The P3HT:PCBM (1:0.7 by weight) blend solution was spin-coated at 900 rpm for 40 sec onto the ZnO layer to form the active layer and baked 90 °C for 10 min. Then, the PEDOT:PSS solution including Triton X-100 (2 wt%) was spin-coated at 4000 rpm for 40 sec onto the active layer, followed by drying at 120 °C for 10 min. Finally, Ag film with 120 nm thickness was deposited by thermal evaporation.

2-4. Characterizations

The size and the morphology of ZnO nanoparticles were analyzed by transmission electron microscopy (TEM, JEOL JEM-2100). The ZnO dispersed 1-butanol was placed on the TEM grid and then dried in drying oven. Dynamic light scattering (DLS, Malvern, Zetasizer Nano ZS) was used to investigate the size of ZnO nanoparticles in the dispersion. The light absorbance of dispersions and the transmittance of film were measured with UV-Vis spectrometer (Agilent 8435, Agilent Technologies). Field emission scanning electron microscopy (FE-SEM, FEI Helios NanoLab 650) was used to observe the surface morphology of ZnO films. The surface roughness of ZnO thin

films was observed in 10 μm × 10 μm area using a non-contact mode atomic force microscopy (AFM, Park Systems, XE-100). After the fabrication of inverted OPV cells, the current density-voltage (J-V) curves were measured by using a Keithley 2400 source-measure unit. The photocurrent was obtained under illumination from an Oriel 3A solar simulator (AM 1.5 G). The illumination intensity was calibrated with a Si cell (VLSI standards, Oriel P/N 54450V). The light intensity used in this work was 100 mW/cm^2.

3. Results and Discussion

3-1. Effect of ZnO morphological properties attributed to the amount of water

Fig. 2 shows the TEM images of ZnO nanospheres and nanorods prepared under different conditions. Without the addition of water into reaction medium, nanospheres with 4 nm are shown in Fig. 2(a). To grow into the nanorods, water was added into the reaction medium because a small amount of water was found helpful to increase the ZnO nanocrystal growth rate [24]. The size of ZnO nanoparticles was increased as amount of water increased compared with Fig. 2(a), while there was no morphological change as a result of low water content as in Fig. 2(b) and (c). Depending on the amount of added water, nanospheres with a diameter ranging from 5 to 8 nm can be obtained. As shown in Fig. 2(d), more than 3 ml water was needed to grow the nanorods. With the addition of water into the reaction medium, the length of nanorods was increased from 18 to 25 nm with high uniformity as shown in Fig. 2(d), (e), and (f). The amount of added water into reaction medium was increased from 1 to 5 mL; the particle

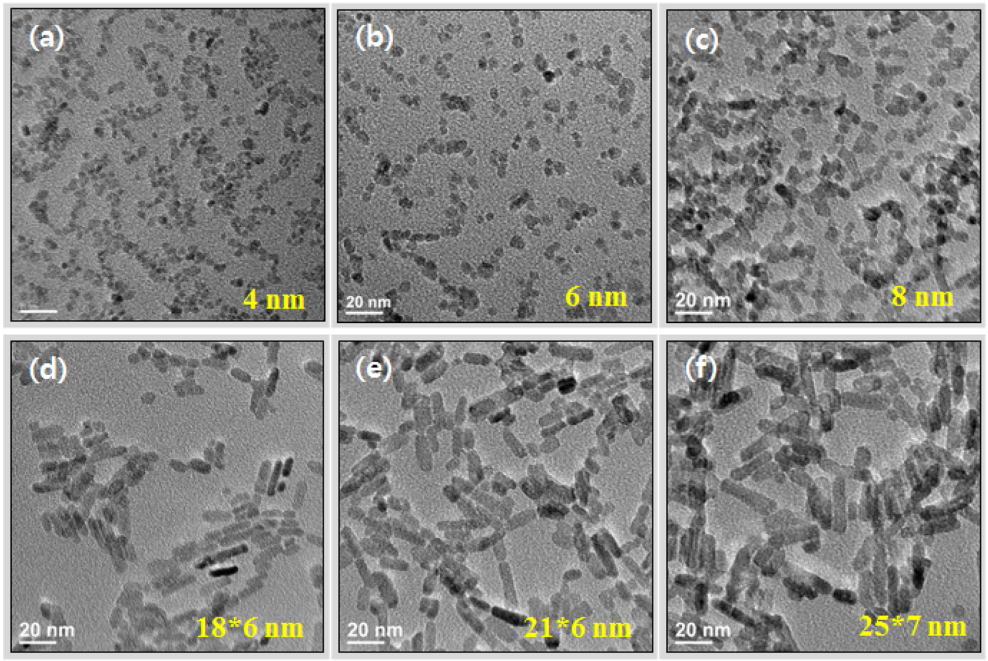

Fig. 2. TEM images of ZnO nanoparticles with different water content: (a) no water, (b) 1 ml, (c) 2 ml, (d) 3 ml, (e) 4 ml, and (f) 5 ml.

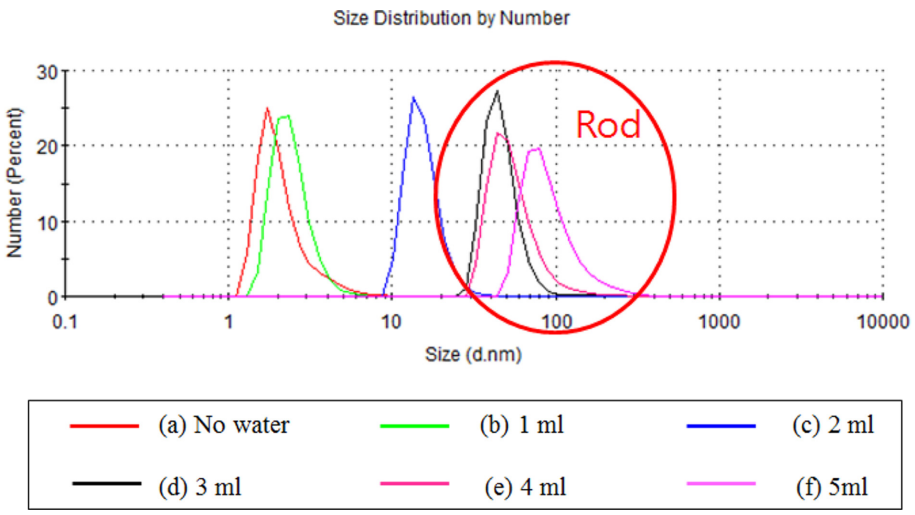

Fig. 3. DLS data of ZnO nanoparticles dispersed in 1-butanol with different water content: (a) no water, (b) 1 ml, (c) 2 ml, (d) 3 ml, (e) 4 ml, and (f) 5 ml.

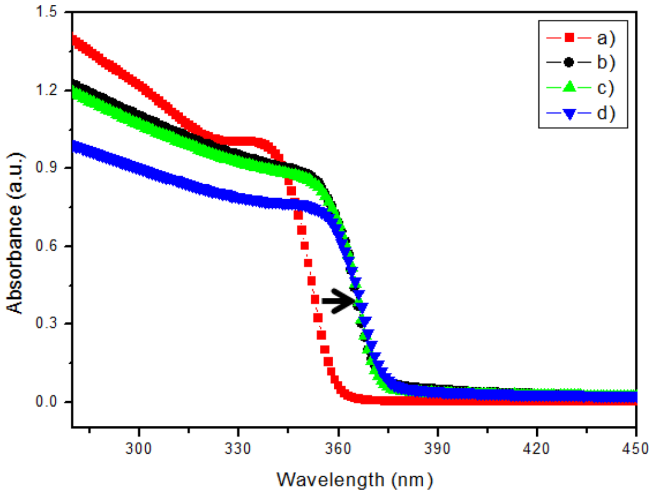

Fig. 4. UV-visible absorption spectra of ZnO dispersion with different water content: (a) no water, (b) 3 ml, (c) 4 ml, and (d) 5 ml.

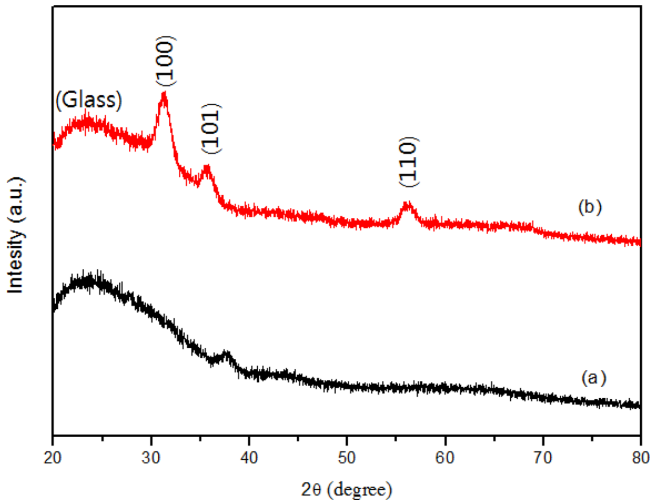

Fig. 5. XRD patterns of ZnO (a) nanospheres (no water) and (b) nanorods (added 5 ml of water) deposited on glass substrate after drying at 200 °C for 2 min.

size was increased with high uniformity. Fig. 3 shows DLS data in a good agreement with TEM images (Fig. 2(a), (b), and (c)) for no water and small amount of water added. However, when water added was more than 3 ml, ZnO dispersions were more opaque according to time passed. This means that there were a few agglomerates. The size distribution of agglomerates in these specimen shows a distribution centered around 50 nm. These results indicate that ZnO existed as an agglomerate structure, consisting of two or three particles, and it is explained by Fig. 3(d), (e), and (f). Also, as shown in Fig. 4, UV-visible absorption spectra could confirm that size of the ZnO particles was increased with water added. It is known that the strong excitonic absorption at ~380 nm has a red shift with the addition of water. This clear red shift in the absorption peak is due to the aggregation of

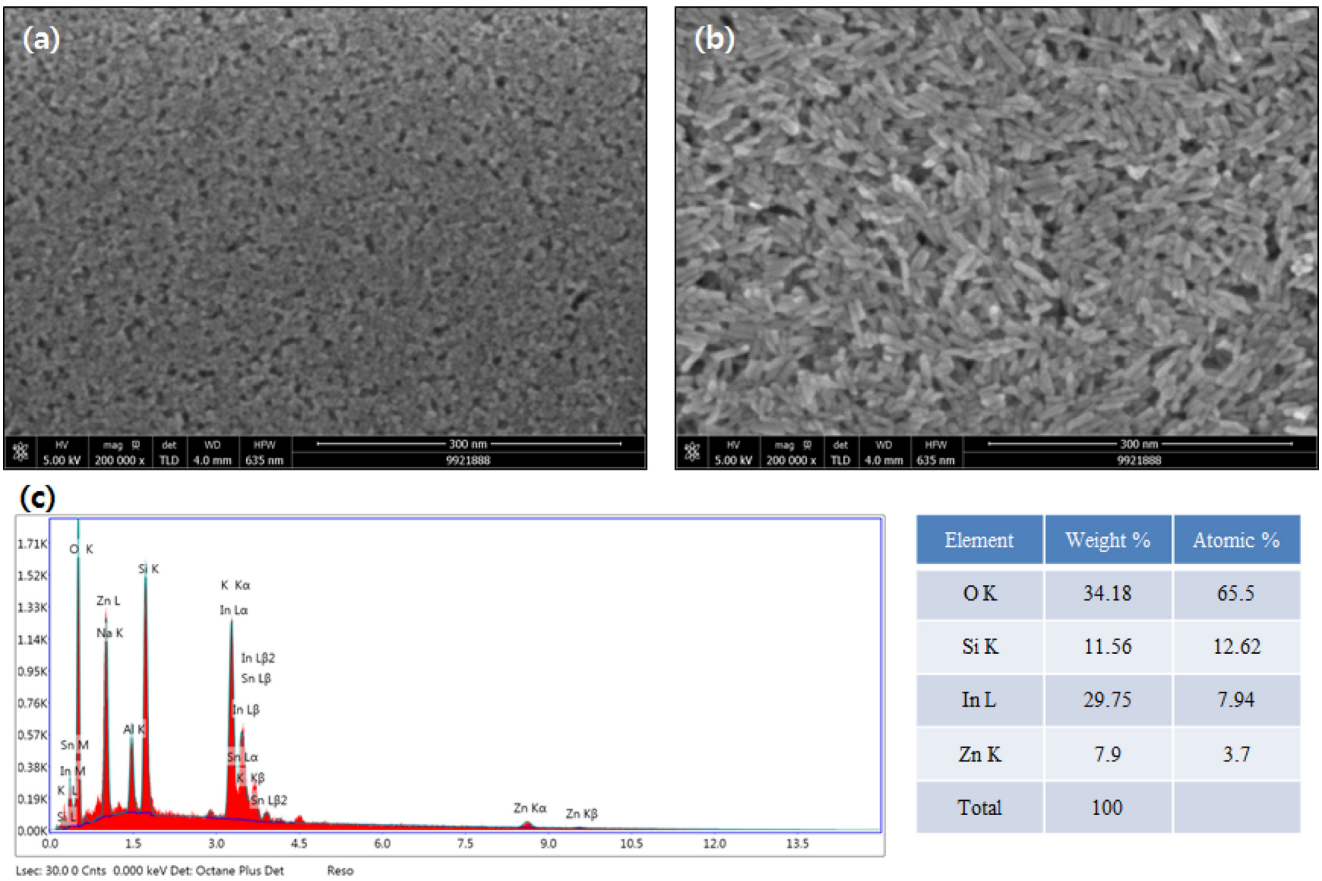

Element	Weight %	Atomic %
O K	34.18	65.5
Si K	11.56	12.62
In L	29.75	7.94
Zn K	7.9	3.7
Total	100	

Fig. 6. SEM images of ZnO films deposited on ITO glass substrates using different particles: (a) nanospheres (no water) and (b) nanorods (added 5 ml of water) after drying at 200 °C for 2 min. (c) EDS spectrum of nanorods.

the particles [25]. Fig. 5 shows XRD patterns of the ZnO films. Fig. 5(a) indicates the particle size is so small and film thickness was so thin that it seems like amorphous nature. As shown in Fig. 5(b), the diffraction patterns of the samples exhibit all the characteristic peaks of the hexagonal wurtzite structural ZnO, according to JCPDS cad no. 36-1451. No other peaks from impurities were detected, which suggests that only single phase ZnO had formed. Representative SEM images of such as-formed ZnO films deposited using different particles are shown in Fig. 6(a), and (b). The images clearly show that flat surface of film was obtained without defect. Following the ZnO film deposition, a drying process was performed at 200 °C for 2 min under air to densify the structure and remove the organic fraction of the film. The interface of the ZnO nanorods was larger than that of ZnO nanospheres, resulting from morphological properties. That is why efficient electron transport of ZnO nanorod layer could reduce the leakage current. To estimate the composition of the as-grown nanorods, EDS analysis was performed. Fig. 6(c) demonstrates the typical EDS analysis of the as-grown ZnO nanorods. It was confirmed that the grown nanorods are composed of Zn and O elements only. Si and In elements may have resulted from ITO glass substrates.

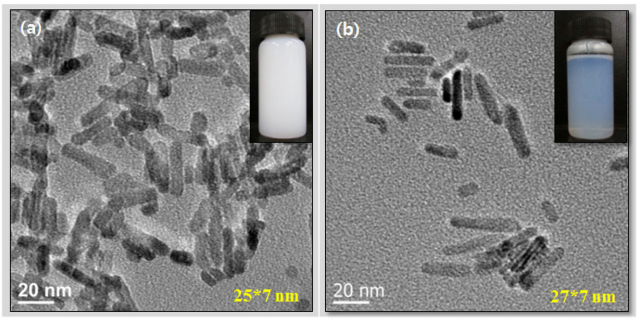

Fig. 7. TEM images of ZnO nanorod synthesized using 5 ml of water (b) with NH_4OH. The inset presents photographs of ZnO dispersion.

3-2. Influence of colloidal dispersion stability

Spherical dispersion exhibits a high stability, and their size and shape maintain at approximately >90% of their original values even after storage for 90 days. However, nanorod dispersions form gel after 1day, depending on the amount of water. The sol-gel synthesis of metal oxides can be performed via the hydrolysis and condensation of metal cations. When hydrolysis rates are faster than condensation rate, gelation occurs [26]. We suppose that addition of water for nanorods increases the hydrolysis rate. Inset of Fig. 7(a) shows optical photograph of 1-butanol solution of the ZnO nanorods, which is opaque dispersion formed gelation. After the addition of NH_4OH to solve this problem, nanorod dispersions did not form gel, as shown in inset of Fig. 7(b). Also, the NH_4OH shifted the pH of the solution towards alkaline deposition, which resulted in accelerated rate of

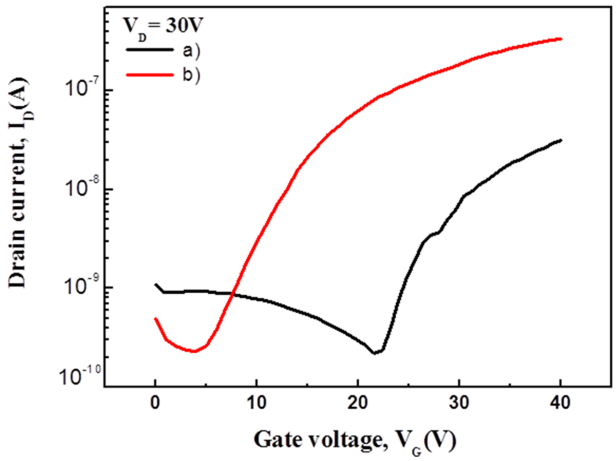

Fig. 9. Transfer characteristics (I_D-V_G) of TFTs fabricated with (a) ZnO nanospheres (no water) and (b) nanorods (added 5 ml of water with NH_4OH).

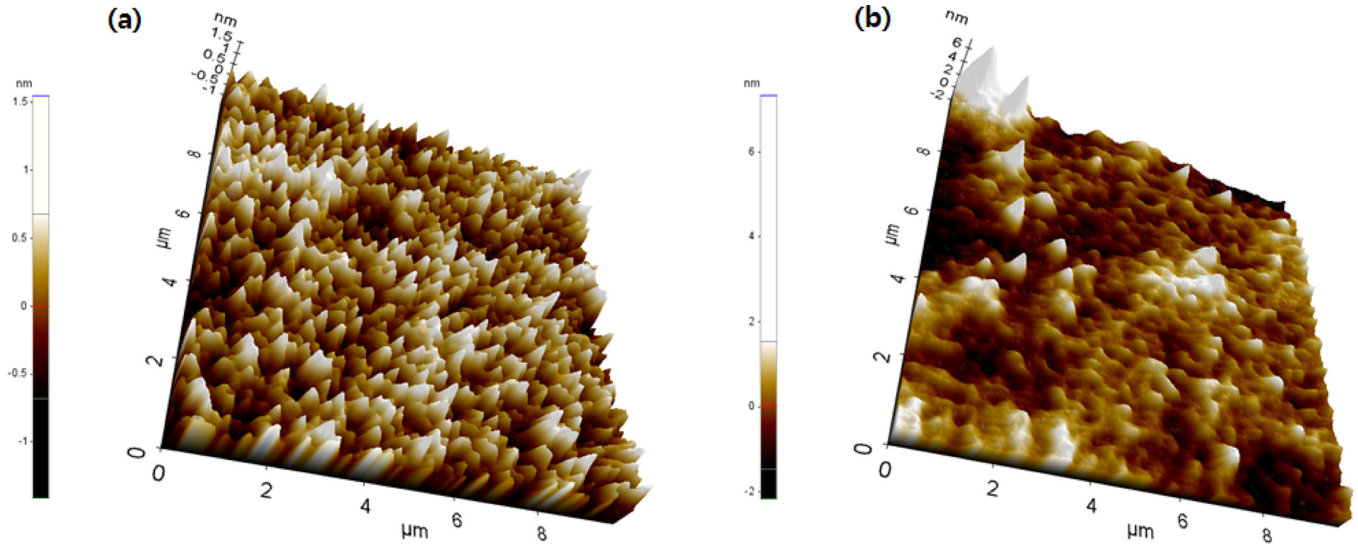

Fig. 8. 3D AFM images of ZnO (a) nanospheres (no water) and (b) nanorods (added 5 ml of water with NH_4OH) deposited on ITO/glass substrates. The rms roughnesses over the 10 μm×10 μm areas are 0.38 and 0.77 nm, respectively.

condensation than hydrolysis. This favors agglomeration of larger particles, as shown in Fig. 7(b) [27]. Fig. 8 shows the surface roughness variation as morphology of ZnO nanoparticles. The ZnO nanosphere film was considerably smoother with a root-mean-square (rms) surface roughness (R_{rms}) of 0.38 nm. The ZnO nanorod film was relatively high R_{rms} of 0.77 nm due to large particle size. The difference in the film morphologies can be correlated with the particle shape. This film having rough structure, leading to lower leakage current due to the improvement in hole blocking capability and electron collection efficiency, enhanced the device performance [28]. Fig. 9 shows current-voltage characteristics of TFT fabricated by using ZnO with two different particles as the semiconducting layer. The I_D-V_G curves reveal that the on/off current ratio of TFT with ZnO nanorods is larger than that of TFT with ZnO nanospheres, and the ratio is higher than 10^3. The extracted field effect mobility of TFT with ZnO nanorods is calculated to be 1.0×10^{-3} cm^2/Vs, which is higher than that of TFT with nanospheres (2.9×10^{-4} cm^2/Vs). This electron mobility difference in ZnO films is caused by the increased interfacial area as morphology of ZnO nanoparticles was controlled. Definitely, mobility of this ZnO film used as inter layer between the active layer and ITO electrode in inverted OPVs for electron extraction and transportation will affect the photovoltaic performance of resulting inverted OPVs.

Fig. 10 shows the current-voltage characteristics under 100 $mW\cdot cm^{-2}$ of the inverted organic photovoltaic cells processed from ZnO nanoparticles of various parameters. The corresponding photovoltaic parameters are summarized in Table 1. Clearly, the device performance is enhanced significantly by highly stable ZnO nanorods film. The inverted device fabricated from ZnO nanosphere film without addition of water exhibits open circuit voltage (V_{oc}) of 0.57 V, short circuit current density (J_{sc}) of 7.94 mA/cm^2, fill factor (FF) of 63.44, and PCE of 2.85%. When using ZnO nanorods film with addition of water (3 mL), PCE of the inverted device was improved to 2.91% with V_{oc} of 0.58 V, J_{sc} of 8.32 mA/cm^2, and FF of 60.8. Also, ZnO dispersion having high uniformity and crystallinity made by increasing addition of water amount to 5 mL and prevented from gelation by using NH_4OH led to both a larger J_{sc} and FF of the inverted device due to their higher electron mobilities and optical transparency [29]. It can be seen that the device performance largely depends on J_{sc}. The J_{sc} of the device is affected by the morphology of particles and stability of dispersion. As shown in Table 1, maximum J_{sc} is obtained with nanorods and addition of NH_4OH. This result indicates that ZnO nanorod increased the interfacial area of the device, leading to more efficient charge collection from device and higher electron mobility compared to nanospheres [30,31].

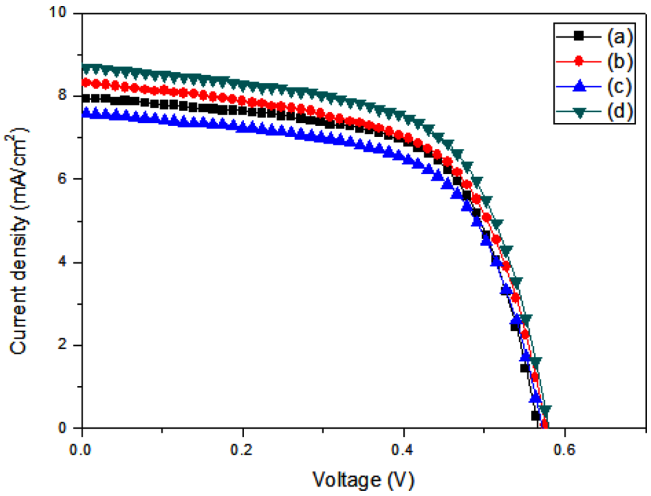

Fig. 10. J-V characteristics of the devices with ZnO nanoparticles from different water content (a) No water, (b) 3 ml, (c) 5 ml, and (d) 5 ml with addition of NH_4OH.

4. Conclusions

Morphology and size of ZnO nanocrystals were controlled from spherical particles to rods with the addition of water in modified sol-gel method and dispersed in 1-butanol for inverted OPVs as an electron transport layer. NH_4OH was added before washing step to prevent gelation of ZnO dispersion. The morphology of ZnO nanoparticles plays an important role in electron transport between the active layer and ITO electrode. Stable ZnO nanorod dispersion by the added NH_4OH showed much better electrical characteristics than ZnO nanosphere dispersion. PCE of device with nanorod film was increased due to the electron mobility of more than three times from 2.9×10^{-4} to 1.0×10^{-3} cm^2/Vs by controlling morphology and size of ZnO particles from spheres. These results indicate that the device performance was strongly dependent on the morphology of ZnO particles and dispersion stability. The optimized inverted OPVs with nanorods demonstrated an enhanced PCE of 16% from 2.68% to 3.12% compared with inverted OPV cell without NH_4OH.

Acknowledgments

This work was supported by the New & Renewable Energy Program of the Korea Institute of Energy Technology Evaluation and Planning (KETEP) grant funded by the Korea government Ministry of Knowledge Economy (No. 20113010010030).

Table 1. Summary of device performance

Device	Shape of ZnO	Amount of water	Addition of NH_4OH	V_{oc} (V)	J_{sc} (mA/cm^2)	FF	PCE (%)
(a)	Spheres	No water	N/A	0.57	7.94	63.44	2.85
(b)	Rods	3ml	N/A	0.58	8.32	60.80	2.91
(c)	Rods	5ml	N/A	0.57	7.56	62.11	2.68
(d)	Rods	5ml	0.5 ml	0.58	8.69	61.91	3.12

References

1. Tan, S., Chen, B., Sun, X., Fan, W., Kwok, H., Zhang, X. and Chua, S., "Blueshift of Optical Band Gap in ZnO Thin Films Grown by Metal-organic Chemical-vapor Deposition," *J. Appl. Phys.,* **98**, 013505(2005).
2. Pearton, S., Norton, D., Heo, K. Y. and Steiner, T., "Recent Progress in Processing and Properties of ZnO," *Progr. in Mater. Sci.*, **50**, 293-340(2005).
3. Kim, H. Y., Jo, Y. K., Lee, K. Y., Lee, I. H. and Tak, Y. S., "Fabrication of ZnO Rod by Electrodeposition and Its Application to Dye Sensitized Solar Cell," *Korean Chem. Eng. Res.,* **50**(1), 162-166(2012).
4. Fortunato, E. M., Barquinha, P. M., Pimentel, A., Gonçalves, A. M., Marques, A. J., Pereira, L. M. and Martins, R. F., "Fully Transparent ZnO Thin-Film Transistor Produced at Room Temperature," *Adv. Mater.*, **17**, 590-594(2005).
5. Bong, H., Lee, W. H., Lee, D. Y., Kim, B. J., Cho, J. H., Cho, K., "High-mobility Low-temperature ZnO Transistors with Low-voltage Operation," *Appl. Phys. Lett.*, **96**, 192115(2010).
6. Çetinörgü, E. and Goldsmith, S., "Chemical and Thermal Stability of the Characteristics of Filtered Vacuum Arc Deposited ZnO, SnO_2 and Zinc Stannate Thin Films," *J. Phys. D: Appl. Phys.*, **40**, 5220(2007).
7. Nair, S., Sasidharan, A., Rani, V. D., Menon, D., Nair, S., Manzoor, K. and Raina, S., "Role of Size Scale of ZnO Nanoparticles and Microparticles on Toxicity toward Bacteria and Osteoblast Cancer Cells," *J. Mater. Sci.: Mater. in Medicine,* **20**, 235-241(2009).
8. Gorla, C., Emanetoglu, N., Liang, S., Mayo, W., Lu, Y., Wraback, M. and Shen, H., "Structural, Optical, and Surface Acoustic Wave Properties of Epitaxial ZnO Films Grown on (0112) Sapphire by Metalorganic Chemical Vapor Deposition," *J. Appl. Phys.*, **85**, 2595-2602(1999).
9. Ravirajan, P., Peiró, A. M., Nazeeruddin, M. K., Graetzel, M., Bradley, D. D., Durrant, J. R. and Nelson, J., "Hybrid Polymer/Zinc Oxide Photovoltaic Devices with Vertically Oriented ZnO Nanorods and an Amphiphilic Molecular Interface Layer," *J. Phys. Chem. B*, **110**, 7635-7639(2006).
10. Krebs, F. C., Thomann, Y., Thomann, R. and Andreasen, J. W., "A Simple Nanostructured Polymer/ZnO Hybrid Solar Cell - Preparation and Operation in Air," *Nanotechnology*, **19**, 424013 (2008).
11. Bouclé, J., Snaith, H. J. and Greenham, N. C., "Simple Approach to Hybrid Polymer/Porous Metal Oxide Solar Cells from Solution-processed ZnO Nanocrystals," *J. Phys. Chem. C*, **114**, 3664-3674 (2010).
12. Chang, P. C., Fan, Z., Wang, D., Tseng, W. Y., Chiou, W. A., Hong, J. and Lu, J. G., "ZnO Nanowires Synthesized by Vapor Trapping CVD Method," *Chem. Mater.*, **16**, 5133-5137(2004).
13. Kong, X. Y., Ding, Y., Yang, R. and Wang, Z. L., "Single-crystal Nanorings Formed by Epitaxial Self-coiling of Polar Nanobelts," *Science*, **303**, 1348-1351(2004).
14. Yang, J., Lin, Y. and Meng, Y., "Effects of Dye Ethching on the Morphology and Performance of ZnO Nanorod Dye-Sensitized Solar Cell," *Korean J. Chem. Eng.,* **30**(11), 2026-2029(2013).
15. Ni, Y. H., Wei, X. W., Hong, J. M. and Ye, Y., "Hydrothermal Preparation and Optical Properties of ZnO Nanorods," *Mater. Sci. and Eng. B*, **121**, 42-47(2005).
16. Spanhel, L. and Anderson, M. A., "Semiconductor Clusters in the Sol-gel Process: Quantized Aggregation, Gelation, and Crystal Growth in Concentrated Zinc Oxide Colloids," *J. Am. Chem. Soc.*, **113**, 2826-2833(1991).
17. Wu, J. J. and Liu, S. C., "Low-temperature Growth of Well-aligned ZnO Nanorods by Chemical Vapor Deposition," *Adv. Mater.*, **14**, 215-218(2002).
18. Marotti, R., Guerra, D., Bello, C., Machado, G. and Dalchiele, E., "Bandgap Energy Tuning of Electrochemically Grown ZnO Thin Films by Thickness and Electrodeposition Potential," *Solar Energy Mater. Sol. Cells*, **82**, 85-103(2004).
19. Saad, L. and Riad, M., "Characterization of Various Zinc Oxide Catalysts and Their Activity in the Dehydration-Dehydrogenation of Isobutanol," *J. Serb. Chem. Soc.*, 73(2008).
20. Rodriguez, J. A., Jirsak, T., Dvorak, J., Sambasivan, S. and Fischer, D., "Reaction of NO_2 with Zn and ZnO: Photoemission, XANES, and Density Functional Studies on the Formation of NO_3," *J. Phys. Chem. B*, **104**, 319-328(2000).
21. Liu, X., Wu, X., Cao, H. and Chang, R., "Growth Mechanism and Properties of ZnO Nanorods Synthesized by Plasma-enhanced Chemical Vapor Deposition," *J. Appl. Phys.*, **95**, 3141-3147(2004).
22. Beek, W. J., Wienk, M. M., Kemerink, M., Yang, X. and Janssen, R. A., "Hybrid Zinc Oxide Conjugated Polymer Bulk Heterojunction Solar Cells," *J. Phys. Chem. B*, **109**, 9505-9516(2005).
23. Li, C. Y., Wen, T. C., Lee, T. H., Guo, T. F., Lin, Y. C. and Hsu, Y. J., "An Inverted Polymer Photovoltaic Cell with Increased Air Stability Obtained by Employing Novel Hole/Electron Collecting Layers," *J. Mater. Chem.,* **19**, 1643-1647(2009).
24. Sun, B. and Sirringhaus, H., "Solution-processed Zinc Oxide Field-effect Transistors Based on Self-assembly of Colloidal Nanorods," *Nano Lett.*, **5**, 2408-2413(2005).
25. Bacsa, R., Kihn, Y., Verelst, M., Dexpert, J., Bacsa, W. and Serp, P., "Large Scale Synthesis of Zinc Oxide Nanorods by Homogeneous Chemical Vapour Deposition and Their Characterisation," *Surf. Coat. Technol.*, **201**, 9200-9204(2007).
26. Livage, J., Henry, M. and Sanchez, C., "Sol-gel Chemistry of Transition Metal Oxides," *Prog. Solid State Chem.*, **18**, 259-341(1988).
27. Bu, I. Y., "Effect of NH_4OH Concentration on P-type Doped ZnO Film by Solution Based Process," *Appl. Surf. Sci.*, **257**, 6107-6111(2011).
28. Sekine, N., Chou, C. H., Kwan, W. L. and Yang, Y., "ZnO Nanoridge Structure and its Application in Inverted Polymer Solar Cell," *Organic Electronics*, **10**, 1473-1477(2009).
29. Yin, Z., Zheng, Q., Chen, S. C. and Cai, D., "Interface Control of Semiconducting Metal Oxide Layers for Efficient and Stable Inverted Polymer Solar Cells with Open-Circuit Voltages over 1.0 Volt," *ACS Appl. Mater. & Interf.*, **5**, 9015-9025(2013).
30. Olson, D. C., Lee, Y. J., White, M. S., Kopidakis, N., Shaheen, S. E., Ginley, D. S., Voigt, J. A. and Hsu, J. W., "Effect of Polymer Processing on the Performance of Poly(3-hexylthiophene)/ZnO Nanorod Photovoltaic Devices," *J. Phys. Chem. C*, **111**, 16640-16645(2007).
31. Baxter, J. B. and Schmuttenmaer, C. A., "Conductivity of ZnO Nanowires, Nanoparticles, and Thin Films Using Time-resolved Terahertz Spectroscopy," *J. Phys. Chem. B*, **110**, 25229-25239(2006).